ARCNL

ADVANCED RESEARCH CENTER FOR NANOLITHOGRAPHY

UTRECHT UNIVERSITY

Photoluminescence and electronic spectroscopy in metal-oxide thin films, with the prospect of application in extreme-ultraviolet lithography

by

Luuk ten Tusscher

Student number: 3473619

in the

Advanced Research Centre for NanoLithography

Supervisors:

Fred Brouwer & Bruno Martins

August 2017

Contents

List of Figures

Abbreviations

CARs	**C**hemically **A**mplified **R**esists
PAG	**P**hoto **A**acid **G**enerator
UV	**U**ltra **V**iolet
EUV	**E**xtreme **U**ltra **V**iolet
ReRAM	**R**esistive **R**andom **A**cces **M**emory
PL	**P**hoto **L**uminescence
CL	**C**athodo **L**uminescence
PLD	**P**ulsed **L**aser **D**eposition
PVD	**P**hysical **V**apor **D**eposition
ALD	**A**tomic **L**ayer **D**eposition
MOCVD	**M**etal-**O**rganic **C**hemical **V**apor **D**eposition
QCM	**Q**uartz **C**rystal **M**icrobalance
XRD	**X**-**R**ay **D**iffraction
AFM	**A**tomic **F**orce **M**icroscopy
PFT	**P**eak **F**orce **T**apping
TM	**T**apping **M**ode
VUV	**V**acuum **U**ltra **V**iolet
CCD	**C**harged **C**ouples **D**evice
CW	**C**ontinuus **W**ave
TEM	**T**ransmission **E**lectron **M**icroscopy
SEM	**S**canning **E**lectron **M**icroscopy
κ	Dielectric Constant
V_O	Oxygen vacancy

Chapter 1

Motivation

For over 50 years the semiconductor industry has followed Moore's law, the biannual doubling of the number of transistors per chip[1]. This progression has been driven by two factors: increasing the size of the chip, decreasing the size of the individual features. Initially the up-scaling of chip size was a large driving force, but in the last few decades all the focus has been on scaling down the individual features. The practice of scaling down is however, reaching its limits. Since the early 2000s, when transistor size dropped below 100 nm, it became more and more likely for electrons to 'leak' from the transistors. So for further down scaling, advances needed to be made in materials and manufacturing techniques. This didn't impede the rate of further down scaling as much and transistor sizes are now in the 10 nm range. It did however influence the costs and the next generation of transistors might be the first generation that is more expensive (in cost per transistor) than its predecessor. The 2015 report of 'The International Roadmap for Semiconductors', which was released in July 2016, claims that the conventional 2D scaling of transistors is coming to an end around 2021. This has forced research priorities in the electronics business to shift to a more device-centric approach, where the focus is on capability integration and reducing power consumption. The modern cellphone is a typical example of this approach, where for instance the image sensor is directly integrated into a digital signal processor. Of course the down scaling of transistors will continue as much as physically possible, but now that the economic incentive is decreasing it will not be the industries' top priority. The main method of producing transistors on chips is by photo-lithography. Lines are 'written' on silicon, which are then connected by gates.

The gate voltage then controls whether the transistor will pass a signal (1) or not (0). Of course there are more complex elements on an actual computer-chip, but this is the basic unit. The 'writing' process is what we are actually interested in. In figure 1.1, the process is schematically shown. First, a silicon substrate with a layer of silicon oxide is spincoated with a photo-resist. The photo-resist acts similarly to a classical photograph, light interacts with the layer causing chemical change. The sample is then treated to dissolve the exposed resist (a positive re-

FIGURE 1.1: Schematic of the lithography process. From top top bottom: Si substrate with SiO$_2$ layer and spin-coated photoresist, exposure, development and etching.

sist) or to dissolve the unexposed resist (a negative resist). We treat the sample, etching the exposed silica, and washing away the remaining photo-resist. Now we are left with a patterned sheet of silica, ready for further production. In this process there are many extra steps like spin coating and baking; and the sample is exposed multiple times. All-in-all a full production cycle contains about 180 steps.

The focus in our research is on photoresists, the light absorbing layer that coats the silica. In current manufacturing, the use of chemically amplified resists (CARs) is most widespread. These are most commonly polymers with a photoacid generator (PAG) that causes the solubility change. CARs have been the dominant type of photoresist since the 1980s, when the exposure was done with mid/near-UV light. And when the industry advanced to using 193nm light, a new generation of CARs enabled the shrinking of feature sizes. This 193nm technology is what is found in today's laptops and smartphones. In recent years however, the industry is exploring technology using extreme UV (EUV) light with a 13.5nm wavelength. And with this new light, come new demands on photoresists. The problem with the now traditional CARs is very fundamental. The diffusion of the PAG causes a further blurring of the picture. Also the EUV source produces far fewer photons per power than the DUV, which causes sensitivity issues. For this reason the industry set out to find a different kind of photoresist. The main requirements are high EUV absorption, small individual unit sizes and an effective mechanism that causes solubility change. That is why currently there is a great amount of research in metal-oxide-containing clusters and nanoparticles, with a metal oxide core and organic ligands. The solubility change is then most likely caused by bond cleavage or ligand exchange,

although little about these mechanisms is understood in the context of EUV lithography. And even though it has been shown that these new photoresists can produce excellent results in EUV lithograpy, the fundamental understanding is not the primary interest of companies. In this thesis we explore the properties of bulk metal-oxides, which are currently under investigation for use in the newest photoresists: Tin (Sn), Hafnium (Hf) and Zirconium (Zr). After illumination and development it is expected that the organic material is largely removed and we are left with the bulk metal oxide, making it an important topic of investigation. By physical deposition methods we will deposit films of which we will study the structural and luminescent properties. Although it is difficult to relate electronic properties of bulk materials to the corresponding nanoparticles, due to quantum size effects and the relative size-to-volume ratio, we also try to draw some parallels between bulk and nanoparticle. The ultimate goal is being to determine what exactly happens when an EUV photon impinges on a photoresist and causes a solubility change.

Even though our primary interest is on photoresists, the materials discussed here are found in a wide range of applications. Tin-dioxide is the most commonly used material in gas sensors and ZrO_2 is also found in this application. More akin to our interests, ZrO_2 and HfO_2 are prospective candidates in the development of new Resistive Random Access Memory (ReRAM). These materials have a very high dielectric constant κ and their optical and transport properties are highly dependant on the amount of defects in the material. As we will see, luminescence is one of the best methods of studying defects and the discussion of defects will play a large role in this work. Because of the high dielectric constant, these materials are also used as gate dielectrics. Because the gate size thickness is dropping below 10 Å, a high dielectric constant is needed simply to contain the electrons. These materials are also found in solar cells, electrodes, catalysts, batteries and the list goes on.

In this thesis we will synthesize these three materials, SnO_2, ZrO_2 and HfO_2. We use physical deposition methods to deposit films of approximately 100nm of the bulk material, which we will characterize in a number of ways. The eventual goal is to relate structural, physical and electronic characteristics to results found in luminescence measurements (Photoluminescence (PL) and cathodoluminescence (CL)). First we will discuss the state of research on these materials by presenting previous papers about the

synthesis of the material, luminescent properties and conclusions stemming from experimental and theoretical work. Then we will briefly introduce the experimental methods that were used, followed by the results and discussion.

The downscaling of features in optical lithography has become very demanding. With the decrease of the wavelength of the incoming photons, the brightness of light sources has become a problem. EUV lithography provides the best resolution to date, but it is very slow. This limited brightness causes the resist sensitivity to put a limit on throughput. The interconnection of these parameters is introduced as the RLS-tradeoff, the interdependence of resolution(R), sensitivity(S) and line edge roughness (LER). LER is usually defined as the 3σ deviation of a line edge from a straight line. In short, it is very difficult to simultaneously get good values on these three parameters. An approximate formula for a certain technological node is: $R^3 L^2 S = Z$. The understanding of the luminescence of these metaloxides is important, because it can provide us more insight into the reactions induced in the ligand stabilized metaloxide nanoparticles. Which in turn can provide us further clues and means to improve the lithography process.

Chapter 2

Introduction

2.1 Electronic transitions in Semi-Conductors

All the materials we are studying in this work are semi-conductors. Although not a requirement, it of course defines the electronic behaviour of the materials. Especially in EUV lithography, where there are numerous secondary electrons, it is important to understand how these electrons interact. A semi-conductor is characterized by having a Fermi level (at room temperature) that is in the small energy gap between the valence- and conduction band (the band gap). The Fermi level at zero temperature is defined as the highest occupied energy level of an electron. At temperatures above zero, thermal excitation allows for electrons to excite to higher energies than the Fermi level. The definition used at non-zero temperatures is then that the Fermi level is the energy level that has a 50% chance of being occupied. If this Fermi level is located in the middle of a band gap, this means that there is an equal amount of electrons and holes (holes are left behind by an electron that is excited to the conduction band) in the conduction and valence band and the material is an intrinsic semiconductor. If this band gap is large, few electrons are excited to the valence band and the material is an insulator. If there is no band gap and the conduction- and valence band overlap, electrons have many available energy levels to occupy and the material is a conductor.

The small band gap allows for interesting tunability of semiconductor materials: the conducting properties can be modified by doping and gating. Doping is the incorporation of acceptor or donor atoms in the semiconductor material, which promote the mobility of holes or electrons. Imagine a crystal with sites with X valence electrons, an

acceptor would then need X-1 valence. This leaves one bond unsatisfied, which causes a neighbouring electron to fulfill this task, leaving behind a hole. The process then repeats itself, allowing the hole to act as a charge carrier and leaving our dopant behind with a negative charge. A donor would need X+1 valence, when the extra electron would act as the charge carrier and the dopant becomes positively ionized. Gating uses an electric field to modify the conductivity. An applied field can alter the energy levels available to electrons, thus de- or increasing the conductivity of the semiconductor. This effect, the field effect, is used in almost all transistors in modern electronics.

The most common mechanism that causes luminescence in semiconductor materials is electron-hole pair recombination. In a semiconductor electrons are constantly excited from the valence band to the conduction band, leaving behind a hole. This excitation is most commonly due to thermal energy, but can also be induced by other energy such as photons. The excited electrons then relax back into the ground
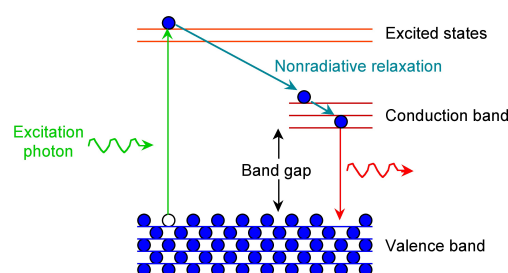

FIGURE 2.1: Schematic representation of the creation of an electron-hole pair and the subsequent relaxation and recombination under emission of a photon.

state and can do so by recombining with a hole and emitting a photon (See figure 2.1). After excitation the electron can interact with photons, phonons, holes and other electrons to facilitate its relaxation. Radiative recombination then usually happens when the electron has reached the bottom of the conduction band. For this reason, the dominant luminescence signal in semiconductor is usually at the energy of the width of the band gap.

In the materials that we study here however, there is significant luminescence at energies below the band gap. This is because there are localized energy levels inside the band gap, that are created by the formation of impurities, or defects, in the crystal lattice. There are various kind of defects that can introduce these energy levels: interstitials, antisite defects and vacancies. An antisite defect occurs in a compound crystal, like a metal dioxide. In this case, on a lattice site where there is supposed to be an oxygen atom, there is now a metal atom or vice versa. Atoms can also be replaced by a contaminant. In Hafnium, for instance, there are always traces of Zirconium and vice versa. A vacancy is exactly what it sounds like, a missing atom on a lattice point. An interstitial

is an extra atom that is not on a lattice site. As we will see, the oxygen vacancy plays a very important role in the electronic structure and luminescence of all the materials that we have fabricated. The neutral vacancy has a doubly occupied one-electron energy level deep in the band gap[2]. The charge distribution can be described as a combination of the four atoms' (Zr, Hf or Sn) bonding orbitals neighbouring the vacant site and it is strongly localized. These sites can then trap an electron or hole, creating the charged vacancy (V^- or V^+). These types of defects have shown to be optically active in various materials and are commonly referred to as farbe(color) centers ($F^{+/-}$). The charged vacancy states can recombine with valence band holes, conduction band electrons or other defects and emit a photon. DFT calculations show that these sites exist and that they can trap electrons or holes. It is however difficult to determine the stability of a charged vacancy state, as the calculations can overestimate the delocalization of electronic states in shallow energy wells and the band gap is also systematically underestimated. For this reason we also cannot reliably assign a theoretical value for the wavelength at which a certain defect-mediated reaction can emit.

2.2   Tin Oxide

SnO_2 is an n-type semiconductor with a 3.6 eV (344 nm) band gap. In the applications mentioned in the introduction, defects play an important role. Films have been synthesized using different techniques. Pulsed laser deposition (PLD) has been used to produce nanocrystalline SnO_2[3][4]. This can be done using a SnO_2 target with a subsequent crystallization process, or using a Sn target with a subsequent oxidation process. Similar results were achieved using thermal evaporation[5]. When films are deposited from a metal target and then oxidized, we see mainly metallic Sn phase until oxidation temperatures of approximately 300°C. Above 300°C, major SnO_2 phase is achieved. This is most likely related to the Sn melting point, which is at 230°C. After treatment at 300°C, the films are mainly in the litharge structure of SnO. After treatments in hotter atmosphere mayor rutile SnO_2 phase is achieved and eventually a denser orthorhombic phase SnO_2, although this orthorhombic is argued to require high pressure[6].

Studying PL in SnO_2 is very interesting, because of the defect structure. As a crystal SnO_2 is almost completely transparent in the visible, but highly conductive (carrier density of $10^{20} cm^{-2}$, comparable to semimetals). It has been postulated for a long time that the reason for this conductivity must be related to shallow donor levels, formed by oxygen vacancies(V_O). However, usually these vacancies form deep energy levels in both

FIGURE 2.2: Unit cells of the litharge structure of SnO (left) and the rutile structure of SnO_2 (right), taken from M. Batzill and U. Diebold[7].

insulators (SiO_2) and semi-conductors (Si). The explanation seems to lie with the multivalency of Sn[8]. Tin oxide has two main oxidation states: stannic tin oxide(SnO_2) and stannous tin oxide(SnO). This makes the formation energy of a tin-interstitial(Sn_i) in a SnO_2 lattice very low, because this leads to a bonding environment that resembles SnO. The presence of Sn_i lowers the formation energy of V_O, explaining the large concentration of V_O that is naturally present in SnO_2. Photoluminescence (PL) was studied in thin films, synthesized using a sol-gel method[9]. It must be mentioned that the crystallinity found in these films was very poor. Two emission bands were found at 400nm and 430nm. The first band was ascribed to electron transitions mediated by oxygen vacancies. There are three different oxygen vacancy charge states: V_O^0, V_O^+ and V_O^{++}. The neutral oxygen vacancy is, as mentioned before, a shallow donor. Therefore it is assumed that most oxygen vacancies are in the singly ionized state. The PL mechanism is then as follows: an impinging photon creates an electron-hole pair, the hole then recombines with the singly ionized oxygen vacancy to produce the doubly ionized state and the state then recombines with an conduction band electron with the emission of a photon. The same group synthesized SnO_2 nanoparticles and found a similar luminescence spectrum[10]. In SnO_2 nanowires and nanobelts luminescence was found at different wavelengths(470nm and 560nm)[11], suggesting that the luminescence may be predominantly caused by surface oxygen vacancies rather than subsurface oxygen vacancies. First principles calculations on the surface of SnO_2 show interesting agreement with experiment, supporting this hypothesis[12].
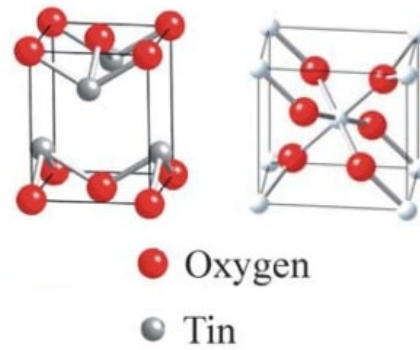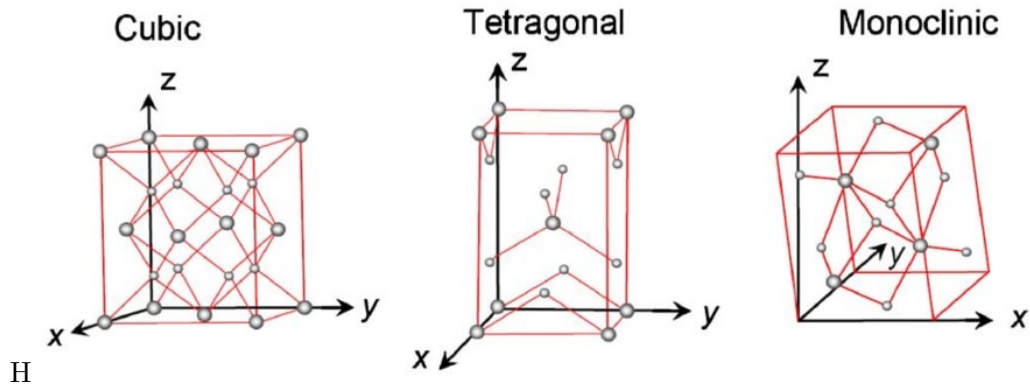
FIGURE 2.3: Crystal structures of zirconia and hafnia, taken from Perevalov et al. [20].

2.3 Zirconia & Hafnia

Zirconia and Hafnia have received increasing amounts of interest in the last several years. Not only coming from industry with regards to use as a dielectric layer, but also because of several interesting properties. These properties are related to the prevalence of oxygen vacancies V_O in these materials. Oxygen vacancies have been shown to cause conductivity[13], while these materials have a very wide bandgap (5-7eV depending on crystal structure), which has (re-)ignited debate about the behaviour of electrons in the neighbourhood of a trap-rich material[14]. Ways to create memory devices, using electrically induced ionic oxygen migration, have also been explored[15]. As mentioned before, zirconia and hafnia nanoparticles are currently being developed as photoresists[16][17][18][19]. The thin film synthesis and structure of zirconia and hafnia have been studied extensively.

Because we use a physical vapor deposition method, the materials are amorphous after deposition. When annealed after deposition both materials crystallize. Both materials have been synthesized in the crystal phases depicted in figure 2.3, but the most stable phase observed at room temperature is the monoclinic phase. At higher temperature these materials can gradually transition into the tetragonal phase. The temperature at which this transformation starts to occur is approximately 500°C, although it greatly depends on the deposition method used[21][22][23][24]. The studies of temperature[25] and oxygen/argon-ratio[26][27] supplied during the deposition process, have shown that oxygen-vacancy-rich films can be synthesized by annealing the films in a low oxygen atmosphere. This can be investigated by the vacancy mediated conductivity, or the photoluminescence.

The relation between oxygen vacancies and photoluminescence has long been accepted in various materials. And also in hafnia and zirconia, various authors have concluded that these vacancies define the PL spectrum. When grown in an oxygen-rich atmosphere, ZrO_2 exhibits a lower photoluminescence intensity than when grown in an oxygen-poor atmosphere[28]. In HfO_2 a similar conclusion was drawn. HfO_2 films were grown and then crystallized in an Argon atmosphere, which increased the PL intensity by two orders. An additional annealing step in oxygen reduced the PL intensity[29]. The luminescence was also studied with regards to the deposition method [30], although without further treatment. The PL bands are the same, but the ratio varies greatly between different deposition methods. All PL bands found for HfO_2 are at 281, 313, 364, 427 and 516 nm, although bands shift and disappear depending on deposition method and treatment. The PL in ZrO_2 and HfO_2 have also been compared using the same synthesis[31], showing very similar spectra.

PL was studied in ZrO_2 nanoparticles [32], finding bands at 353 nm and 492 nm. The 353 nm emission band was attributed to oxygen vacancies, in the same way as in SnO_2. The 492 nm emission was actually assigned to Ti^3 centers. This mechanism is illustrated in figure 2.4. The deep Oxygen vacancy (V_{o2} in the figure) can trap an electron which can then not be thermally released to the conduction band. They instead recombine with a hole and transfer to the ground state, emitting at 353 nm. The Ti^{3+} centers absorb the holes, creat-

FIGURE 2.4: Energy diagram for the luminescence-mechanism in Zirconia. On the left the mechanism mediated by Ti-defects and on the the right the mechanism mediated by oxygen vacancies.[32]

ing a Ti^{4+} center. The recombination of these centers with conduction band electrons, emits the 492 nm emission. One of the main reasons to argue these different mechanisms is because the afterglow properties were studied, where only the emission at 492 nm had longer lasting emission. This is because the Ti^{4+} could recombine with the electrons that were trapped in the shallow oxygen vacancy levels (V_{o1}), that took time to be thermally excited into the conduction band. Interestingly, the duration of the afterglow

was dependant on the temperature at which the material was treated. At 600-1100°C, afterglow could be detected for 30 seconds. While after annealing at 1600°C, afterglow could be detected for around 1000s. In HfO_2 nanoparticles a similar spectrum was found, with emission bands at 414nm and 520nm for pure monoclinic phase[33]. Annealing the nanoparticles increased the crystallinity and the PL, analogous to the thin films. When HfO_2 nanoparticles were synthesized in pure cubic and pure monoclinic crystal phase, a significant difference was shown[34]. Both polymorphs featured the dominant peak at 496nm, but there also was a 400nm peak exclusive to the cubic phase. Furthermore, when the PL was measured for different temperatures an interesting observation was made. When the temperature increased the monoclinic nanoparticles showed a decrease in PL intensity, while the cubic nanoparticles showed an increase[35]. When fitting the data, the curves show a similar activation energy. This suggests that a similar recombination process is involved. Probably the shallow trap level upon thermal depopulation, provides either extra carriers or acts as a non-radiative recombination center.

We can conclude a few things about the PL observed in the metal-oxides discussed above. It is very likely that some of the bands observed are caused by oxygen vacancies. These can be incorporated into the film by annealing in an oxygen-poor atmosphere. The PL spectrum is also highly dependant on the crystallinity and deposition method of the material. Thin film synthesis is also not a trivial task. In this work we will make these thin films and study their luminescent properties, in order to clarify the fundamental mechanisms that partake in these processes.

Chapter 3

Experiments

3.1   Sample preparation

To deposit the material we use physical vapor deposition (PVD) methods. This means that we use a physical process (heating, sputtering) to produce a vapor which deposits onto a substrate. This method is used for the production of solar cells, coating of tools and even for producing balloons. Out of the materials studied here, HfO_2 is by far the most explored in respect to PVD[36][37]. This is because HfO_2 has been a candidate for usage as a gate dielectric and has been in use as such since a few years now. Those works have been focused on including dopants to increase the crystallization temperature, increase electron mobility and increase the drive current. That were the problems, for chip manufacturers, in HfO_2. Theoretically, atomic layer deposition (ALD) and metal-organic chemical vapor deposition (MOCVD) should produce the most uniform films and the thickness should be the most accurately controlled. These are chemical methods and the thickness only depends on the number of reaction cycles, but herein also lies the downside. There is always a risk of residues being left from the precursor and the film purity depends on the completeness of the reaction. These methods are also very expensive. PVD, on the other hand, is conceptually and practically very simple and produces very pure films for very little cost. For these reasons, and of course also because of availability, we use PVD methods in our deposition. As a substrate we use 12x12mm (100)silicon substrates, about a millimeter thick. Before deposition we clean the substrates with base-piranha (a solution of ammonium hydroxide (NH_4OH) with

hydrogen peroxide (H_2O_2)) to remove most organic material and with a 10% hydrogen-fluoride (HF) solution to remove the native oxide layer. The samples were stored in a dessicator with a humidty of 5% H_2O.

3.1.1 tin oxide

To prepare the SnO_2 films, we use a home-built thermal evaporation device nicknamed 'SMURF'. It's a vertical tube of roughly 50 cm high, with an Al_2O_3 crucible containing Sn and a sample holder at the top of the machine with a shutter beneath it. A vacuum pump pumps the system down to 5×10^{-6} mbar before deposition. The crucible is heated by a current of up to 45 A, until a steady deposition rate of about 3 Ås[1] is achieved, measured by a quartz crystal microbalance (QCM). Then the shutter is opened, until we have a film of approximately 100 nm. After the initial deposition, the samples are placed in a tube furnace for two hours at 200°C with an oxygen background pressure to partially oxidize the films. The films are then treated at 500°C for two hours with a background pressure varying from pure Ar to pure O_2, to get different concentrations of oxygen vacancies.

3.1.2 Hafnia and Zirconia

To prepare the HfO_2 and ZrO_2 films, we use another home-built electron beam evaporation device 'KAMELEON' (see figure 3.1). It consists of a large vacuum chamber with two crucibles and two cathodes in the bottom of the machine and a sample holder at the top. The chamber is pumped down to 1×10^{-6} mbar. We then turn on our electron beam, which can be 6 kV or 10 kV and 0-0.5 A. Because Zr
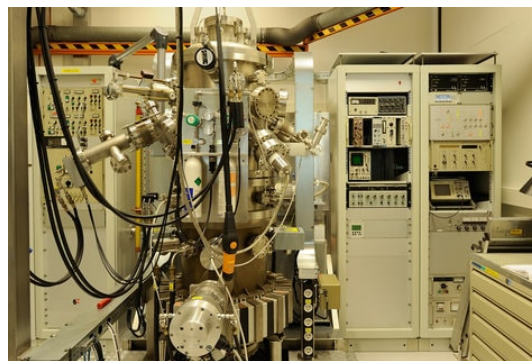

FIGURE 3.1: The KAMELEON e-beam deposition device.

and Hf have very high melting points (1855°C and 2231°C respectively), we need the 10kV beam with maximum current to get an evaporation rate of 2-3Ås[1]. The evaporation rate is again measured with a QCM and we aim for a 100nm thick film. The annealing treatment is slightly different from the SnO_2 treatment. At 200 °C very little

happens, so we immediately anneal at 500°C with varying ratios of O_2/Ar. The ratios of Argon/Oxygen we use are 1/0, 0/1, 0.9/0.1 and 0.57/0.43. The choice of these ratios is not arbitrary. We have seen in the literature[27] that in HfO_2 the grain size decreases with increasing Oxygen pressure up until 20-30% Oxygen[26]. Studying the capacitance-voltage behaviour also revealed a change in behaviour at around 20% Oxygen[27]. So it is logical to take measurements below and above this 'limit'.

3.2 Characterization

To characterize the prepared materials, we have used a number of methods. To characterize the structure we use X-Ray Diffraction, Raman spectroscopy, and Atomic Force Microscopy. The luminescent properties have been studied using two methods: Photoluminescence (PL) and Cathodoluminescence (CL). The principles of each technique will be briefly introduced in the following sections.

3.2.1 X-Ray Diffraction

X-Ray Diffraction (XRD) is based on the coherent scattering from parallel crystal planes. The material is illuminated by an X-Ray beam, with a varying incident angle. If the material is crystalline to some degree, implying that there are parallel crystal planes, then the X-Rays will scatter
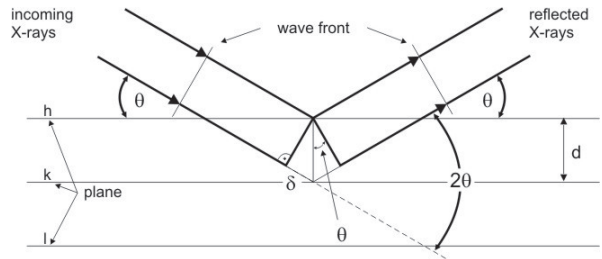

FIGURE 3.2: Schematic picture of Bragg refraction. The incoming X-rays scatter coherently if $sin\theta = \frac{d}{n\lambda}$.

coherently under some angle. This is most commonly known as Bragg's law or Bragg diffraction (see figure 3.2). For this we use a Bruker D2 Phaser.

3.2.2 Raman Spectroscopy

In Raman spectroscopy, monochromatic light in-elastically scatters and returns information about the chemical bonds in the material. We detect phonons (lattice vibrations) and molecular vibrations with the backscattered light. The incoming beam excites the

molecule into a higher rotational and/or vibrational virtual state, before returning an inelestically scattered photon. For Raman spectroscopy we use a WITec confocal raman microscope, with 532nm excitation-light.

3.2.3   Atomic Force Microscopy

Atomic Force Microscopy (AFM) is a relatively new technique (1982), that is used to image surface topology. An AFM consists of a cantilever with a very sharp tip, controlled by piezoelectrics that facilitate tiny and accurate movements. The tip is often made of silicon or silicon-nitride with a tip radius of a few nanometers. The tip is brought into proximity of the surface, when the forces between sample and tip cause the tip to deflect. The deflection is measured by a photodetector, that measures the reflection of a laser of the back of cantilever. There are many forces that can be probed in such a manner, by varying the imaging mode or the tip functionalization. The imaging mode we use in this work is Peak Force Tapping (PFT), which is very similar to Tapping Mode (TM). In TM the cantilever oscillates at (or near) its resonance frequency and due to interaction with the sample the amplitude and frequency of this oscillation changes. Detected changes in cantilever amplitude and oscillation frequency are corrected to a setpoint value by actuating the cantilever in Z via a feedback-controlled piezo. These correction voltages sent to the Z piezo are recorded and correlated to a voltage-distance calibration factor in order to determine the height at a given XY coordinate[38]. PFT is largely similar to TM, but with a few important differences. In PFT the cantilever does not oscillate at its resonance frequency, thus avoiding the dynamics of a resonating system. The trick is then to modulate the z-position with a sine wave instead of a triangular wave to avoid resonances at the turnaround point. PFT refers to the method that uses the individual peak force points as triggering mechanisms to force the z-piezo to retract. The algorithm recognizes the local peak force, even though it is far below the setpoint value. This allows operation at low forces, which increases the resolution especially in soft samples. For this we use a Bruker Icon AFM machine, with standard silicion-nitride tips.

3.2.4 Photoluminescence

To study the energy levels caused by defects in the films we look at their luminescence. This way we can probe electronic defect states in the bandgap Photoluminescence(PL) is light emission induced by photons. Photons excite electrons to higher energies, which go through various relaxation processes in some of which, other photons are emitted. The mechanism we are interested in are the ones where defects mediate these processes. If we consider an acceptor level A^0 and a donor level D^0, after optical pumping electrons and holes will be bound at A^- and D^+ to generate charged centers. We have already seen in the intro the example of the oxygen vacancy absorbing an electron to become a charged emission center. These centers can then recombine: $A^{-X} + D^+X \rightarrow h\nu + A^- + D^+$. A donor or acceptor can also recombine with an electron or a hole to emit radiation: $A^{-X} + h^+ \rightarrow h\nu + A^{-X+1}$ or $D^{+X} + e^- \rightarrow h\nu + D^{+X-1}$.

For the experiment we use a HORIBA vacuum ultraviolet (VUV) setup. This setup consists of a Energetiq EQ99 Laser Driven Lightsource and a Triax 190 monochromator to produce the excitation light. The detection is done by an iHR320 monoch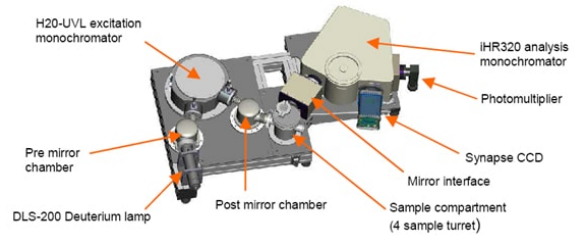romator coupled to a CCD detector (see figure 3.3). Slits with variable widths are placed after the monochromater and before the detector. The incoming beam makes a 90° angle with the direction of the light that goes into the detector and the sample makes a 45° angle with the in- and outgoing beams.

FIGURE 3.3: Schematic of the VUV luminescence setup.

3.2.5 Cathodoluminescence

In cathodoluminescence (CL) we induce the luminescence by illuminating the sample with an electron beam. There are a few key differences with PL, making this an interesting addition. First of all the energy spectrum of an electron beam is very different. If we look at a continuous wave (CW) laser, we have a field oscillating at a a fixed frequency. An electron however, is a point charge with a field evolution that is tightly

bound in space and time. If we take the fourier transform to frequency space, the CW laser provides a single frequency but the electron beam provides a very broad spectrum of energies. Secondly an electron has access to other processes than a photon. Similarly to PL, electrons can excite valence electron to higher energies that lead to electron-hole pairs that can radiatively recombine. The broad range of the electron energy spectrum should however provide access to more excitation modes. Additionally there are coherent processes, where there is a fixed phase relationship with the fields of the incoming electrons. The main sources of coherent radiation are: Cherenkov radiation, transition radiation, diffraction generation and plasmon generation. Cherenkov radiation is emitted when the electron phase velocity exceeds the speed of light in the material, this causes the characteristic blue glow in nuclear reactors. Transition radiation is the much more general case where an electron crosses the boundary of two materials with different dielectric constants. This causes an induced field, leading to surface currents and charges that radiate into the far field. Diffraction generation occurs when an electron travels close by (not through!) a structured surface like a grating. Finally the electric field of the electron can couple to a plasmon resonance. The field can only do work in the direction parallel to the incoming field, which in this case is the vertical direction because the TEM is vertically oriented. So electron beam excitation is very sensitive to vertically oriented modes. This is why CL is used to study surface plasmon polaritons in metals. These coherent processes are of little interest to us however, because we are looking at wide bandgap semi-conductors. In metals, the electronic channels are more dominant while in insulators/semiconductors radiative processes are several orders larger.

The CL setup used was home-built and operated by Dr. Benjamin Berry[39], which is based on a scanning electron microscope (SEM, FEI XL-30) with a Schottky field emission gun electron source. Beam energies are in the range of 1-30keV and the current is between 0.1 and 30 nA. The primary light collection is done by an off-axis parabolic mirror. Measurements with this system are possible on the $\lambda_0 = 360\text{-}1100$ nm range, with sensitivities of 10-15% in the $\lambda_0 = 499\text{-}900$ nm range. This is unfortunately not ideal for our system as luminescence is observed with wavelengths down to 250nm.

Chapter 4

Results

This section is structured the same as the 'Experiments' section. First we will go over the structural properties of the materials investigated by XRD and AFM, followed by the luminescent and electronic properties, studied with PL, CL and Raman-spectroscopy.

4.1 tin oxide

In figure 4.1 we see an AFM picture from the oxidized Sn film. This specific picture is of the film annealed first in a 100% Oxygen environment at 200°C and then in a 10% Oxygen environment at 500°C, but the films annealed at different Oxygen/argon ratios look very similar. The film appears to have a droplet- or pillar-like structure. We believe this to be because of the properties of the deposition device, specifically its size. The device is quite small, so that the heat generated at the crucible influences the temperature of the substrate. So instead of a physical deposition, we have a condensation. We believe that this leads to the clumped structure of the film.
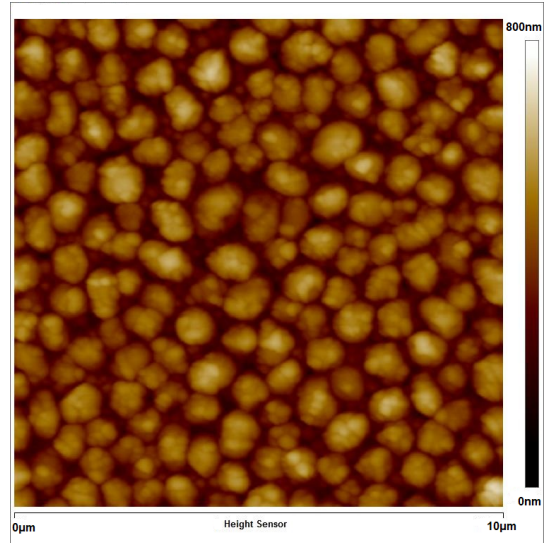
FIGURE 4.1: AFM height image of the tin oxide thin film, after annealing at 200° for two hours in pure Oxygen. The color scale is 0-800 nm and the picture size is 10×10 μm.

This is important to realize, because it also means that the oxidation also does not form a layer of Tin oxide in the plane parallel to the substrate surface. Instead it oxidizes on the surface of the tin droplets.

In the XRD spectrum we can clearly identify different peaks. In figure 4.2 we see the spectra for Tin on Silicon and Quartz, after the first annealing step at 200°C. By comparing with literature [40][3], we can identify the peaks corresponding to metallic Sn (stars) and SnO (solid circles). And comparing the substrates we can see the peak corresponding to the Silicon (100) substrate (empty square). In figure 4.2 and figure 4.3 we see the spectra for the films annealed for the second time at 500°C with varying Oxygen\argon ratios. We can clearly see the formation of SnO$_2$ peaks (blue circles) and the dis-
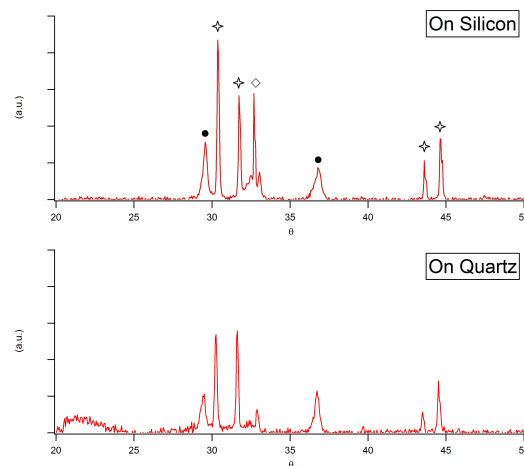

FIGURE 4.2: XRD spectra of the Sn films after annealing at 200°C for two hours with 100% Oxygen pressure. With the top figure Sn deposited on silicon and the bottom figure Sn on Quartz. The peaks correspond to metallic tin (stars), the silicon substrate (empty square) and SnO (solid circles).
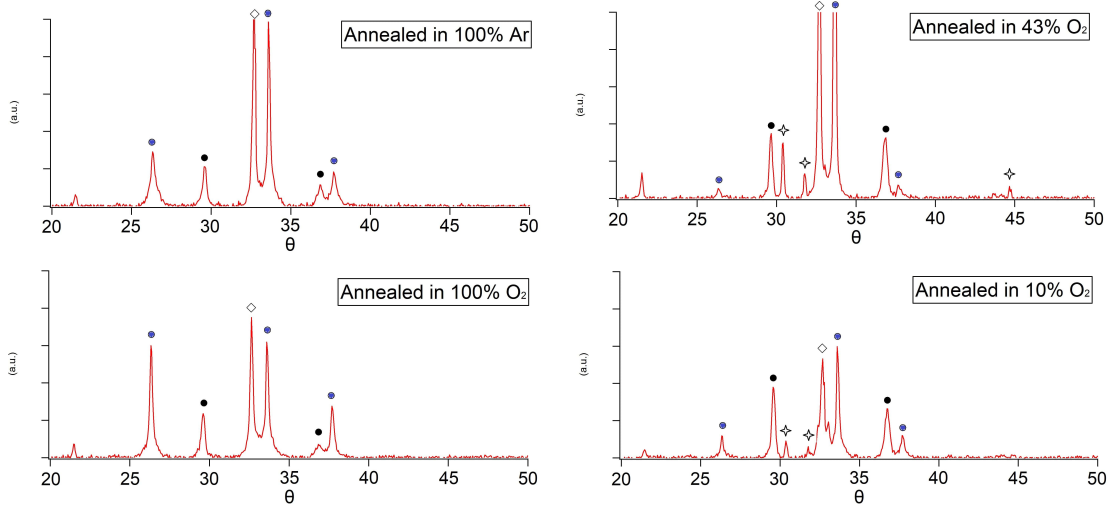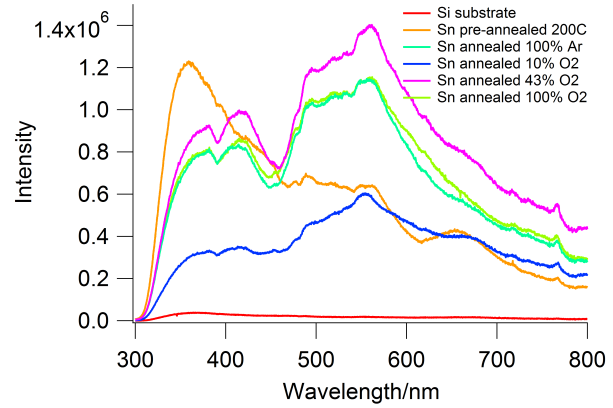
appearance of metallic Sn. There are however some inconsistencies. Especially the sample annealed in 100% argon shows strange results. If we look at the pair of peaks at 37°(SnO) and 38°(SnO$_2$) we can see a progression from the 10%O$_2$ and 43% O$_2$ samples to the 100% O$_2$ sample. The SnO peak gradually decreases, while the SnO$_2$ peak increases. Similarly, in the 10% O$_2$ and 43% O$_2$ samples we can still see peaks of metallic Sn, while those have completely vanished in the 100% O$_2$ sample. There is however an inconsistency between the 10% O$_2$ and 43% O$_2$ samples, where the 10% O$_2$ sample seems to have relatively more SnO$_2$ and less metallic Sn, while we would expect the opposite. Moreover, the XRD of the sample annealed in pure argon looks almost the same as the sample annealed in pure Oxygen, while we would expect it to have the most metallic Sn and the least SnO$_2$.

FIGURE 4.3: XRD spectra of Sn films annealed at $200°C$ for two hours and subsequently at $500°C$ for two hours. On the left the films annealed in 100% argon (top) and 100% Oxygen (bottom). On the right the films annealed in 34% Oxygen (top) and 10% Oxygen (bottom). The peaks correspond to metallic tin (stars), the silicon substrate (empty square), SnO (solid circles) and SnO_2 (blue circles).

The PL spectra of the tin samples are shown in figure 4.4.

To make sure we are not seeing the substrate, we measured a blank substrate (red line) which shows that there is a negligible signal coming from the substrate. The orange line corresponds to the pre-annealed tin and the other lines to samples with further annealing. We can not see a great difference in the shape of the spectrum for the films treated at $500°C$. To find a correlation between the oxygen

FIGURE 4.4: PL spectra of various tin oxide samples annealed at different Oxygenargon ratios. Excitation light is 220 nm with a cutoff filter at 330 nm. Recording time is 30 seconds.

vacancies and their luminescence, we have to see an emission band varying depending on the oxygen concentration used during annealing. But as we have seen in the XRD spectra, the oxygen ratio used during annealing also influences the crystallization and the ratio of SnO_2 to SnO and Sn. As mentioned in the introduction, Gu et al.[9] found emission in tin oxide thin films at 400 and 430 nm. Attributing the 400 nm emission to

transitions mediated by the defect levels in the band gap created by oxygen vacancies. As their films were fabricated using a different method (spin-coating) than we have here, the corresponding bands can slightly differ. Due to compressive stress the band gap can change, shifting emission levels[41]. So it is probable that the first two bands in our spectra, at 380 and 410 nm respectively, correspond to these bands. Emission in the 500-600 nm range has been found in nanobelts[11], where a 600 nm emission band was assigned to surface oxygen vacancies. We must then also conclude that the concentration of oxygen vacancies is not significantly influenced by the annealing atmosphere, as far as we can see from the corresponding emission bands.
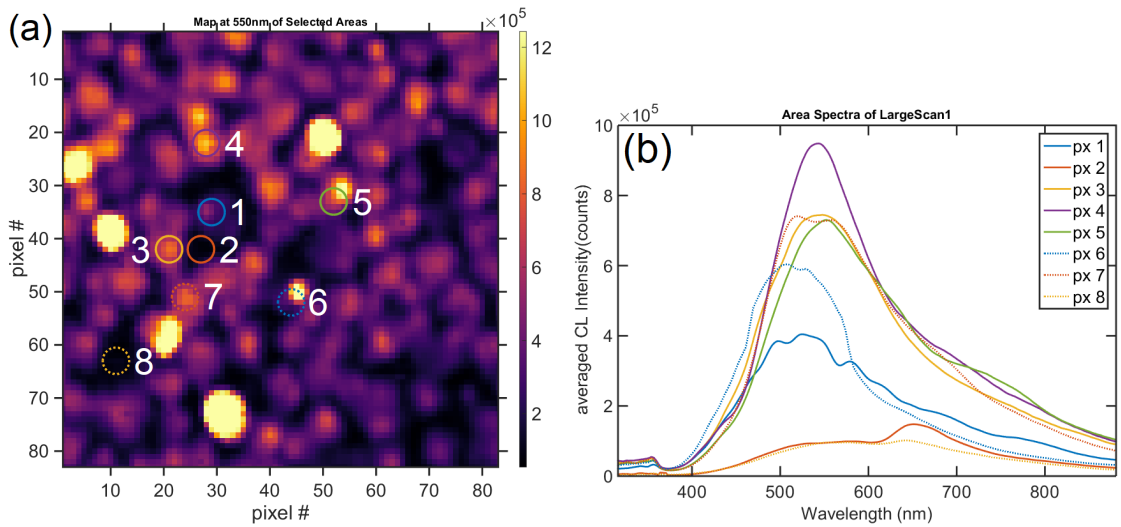

FIGURE 4.5: In (a) CL intensity map for 550 nm light, showing the locations of the taken spectra (9 pixels in each circle) and in (b) the spectrum corresponding to each location. One pixel is 8.64×8.64 nm. The sample used is the SnO_2 sample annealed in the 10% oxygen atmosphere at 500°C for 2h.

In figure 4.5, we see the cathodoluminescence spectra of our tin oxide sample. We can see the pillars from the AFM image, but with varying intensities of luminescence. The spectra taken from the brightest spots (pixels 3, 4, 5 and 7) show an emission band at 550 nm. The spectra taken from edges of luminescent spots or from less intense areas (pixel 1 and 6), show a lower emission at a wavelength of 510 nm. We assume that the varying luminescence intensity corresponds to the relative amount of SnO_2, the intense areas being the areas with the highest amount of SnO_2. Further supporting this claim is micro-raman data, as reported by Sangaletti et al. [40], that shows a similar distribution (or growth) of SnO_2.

Raman spectroscopy was used to identify specific low-energy modes, that are specific to the crystal polymorphs of tin oxide. The problem with these tin films is that due to their thickness we look through the sample at the substrate. In (a) in figure 4.6 we see the spectrum recorded for our SiO_2 substrate after cleaning (this should give it a SiF surface, although that should not be visible), with an accumulation time of five seconds. We see major peaks at 297, 513 and 965 cm^{-1} and minor peaks at 165, 613 and 965 cm^{-1}. If we compare this to the bottom figure, where we have shown the Raman spectra for the various tin oxide samples, we see mostly the same features. This indicates that the film is too thin, and the excitation light penetrates into the substrate. When we subtract the signal from the substrate, we see that the remaining signal shows two peaks. These are shown in figure (c) where the picture is zoomed in on the 100-300 cm^{-1} region. Here we see peaks at 165 cm^{-1} and 208 cm^{-1}. From the literature[40][42] we learn that there are bands at 171 cm^{-1} and 211 cm^{-1} (our bin size is 4.683 cm^{-1}). The 211 cm^{-1} band corresponds to SnO, while the 171 cm^{-1} band corresponds to a substoichiometric SnO_x.
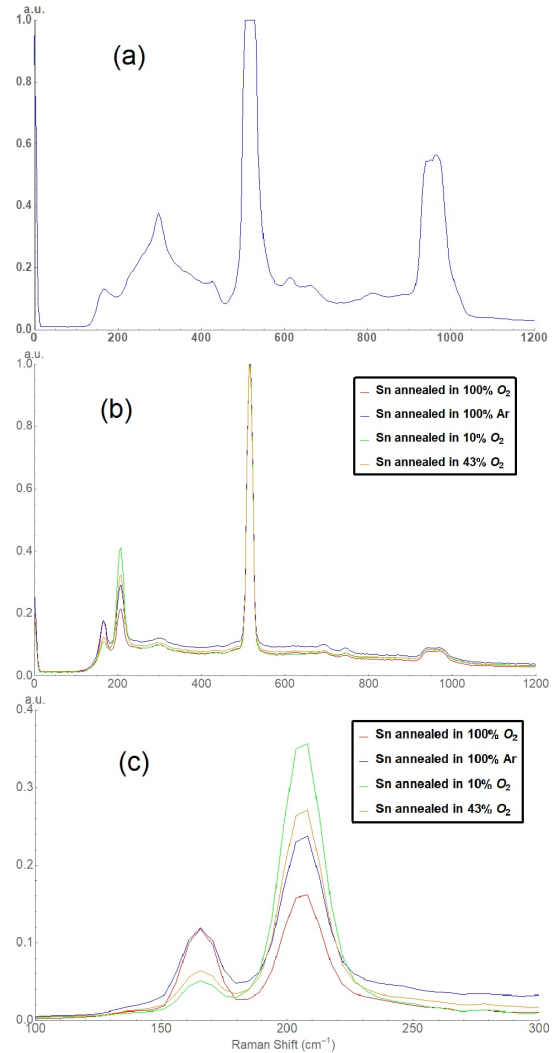
FIGURE 4.6: The Raman spectrum of the Silica substrate (a), from an accumulation time of 5s. The spectra of the various tin oxide samples (b), from an accumulation time of 30s. The region 100-300 cm^{-1}, zoomed in (c), with the background substracted.
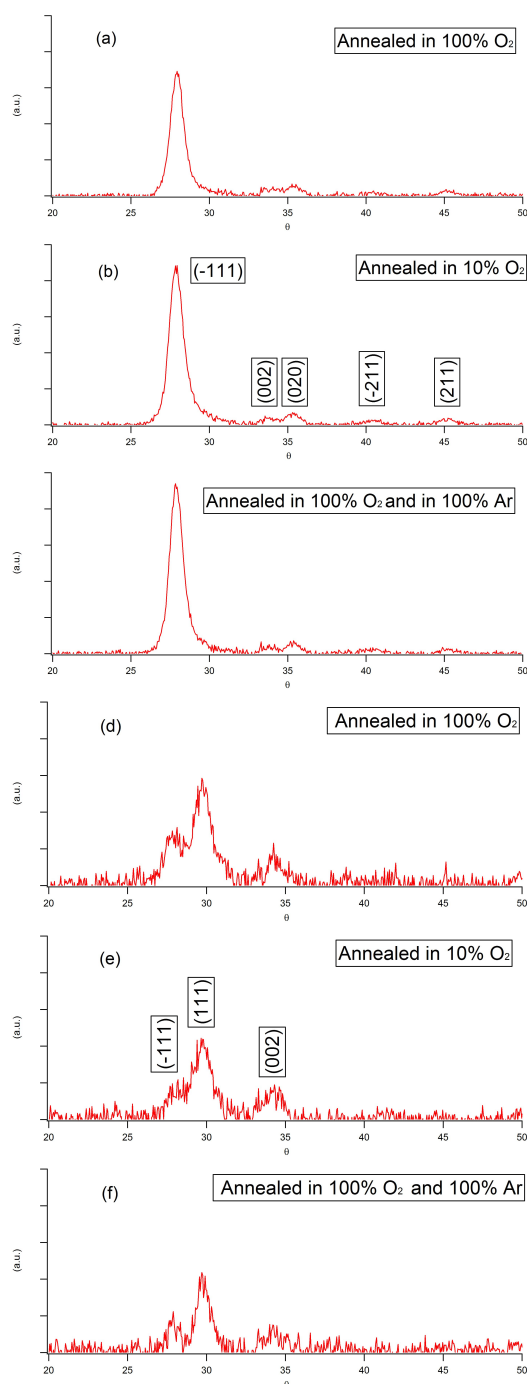
4.2   zirconia

FIGURE 4.7: XRD scans of the hafnia and zirconia samples annealed at 600°C, in varying Oxygen\argon ratios. (a)-(c) are the hafnia samples and the (d)-(f) are the zirconia samples.

The XRD spectra of the hafnia and zirconia films show that they are significantly less crystalline than the tin oxide films. This is to be expected, as these elements have a far higher melting point than tin. The melting point of Sn is at 232°C, while those of zirconium and hafnium are at 1855°C and 2231°C respectively. We can distinguish peaks corresponding to the monoclinic crystal phase for hafnia and tetragonal for zirconia, but between samples there are no significant differences. This indicates that crystallization is primarily driven by temperature, and not by the relative concentration of oxygen and argon during the process, as was discussed in the introduction. This could also be due to suboptimal conditions regarding the purity of the atmosphere during annealing. Of course this does not mean that an Oxygen-poor atmosphere does not induce the formation of Oxygen-vacancy defects.

The PL in ZrO_2 and HfO_2 was excited at 220 nm, with a cutoff filter at 330 nm. Unfortunately this cuts away most of the 250-350 nm region, were several bands have previously been found. We can however distinguish the peak at around 400nm, while the peak we expect to see at around 350 nm is largely cut off. The most interesting observation is made when comparing the different samples. We can clearly see that the 400 nm peak for ZrO_2 emission is relatively larger in the sample an-
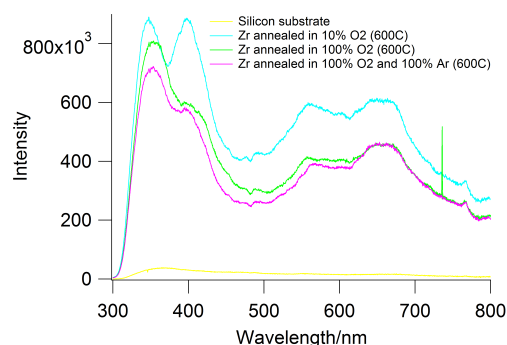

FIGURE 4.8: Photoluminescence spectra of zirconia films annealed in different Oxygen\argon ratios. With excitation at 220 nm and a long-pass filter at 330 nm.

.

nealed in 10% oxygen. This peak has been observed by other authors in sol-gel derived ZrO_2 films[43][44], although the films showed very similar XRD spectra. The authors assigned the band to the neutral and singly excited oxygen vacancy, referring to DFT[2]. The shift in emission energy can again be due to the band gap being lowered by a difference in stress. In films grown by ion-beam sputtering, the emission peak was found at 435 nm[28]. Once again the authors assign the emission to oxygen vacancies (although no specific state), by comparing photoluminescence excitation with a calculated absorption spectra. This seems to confirm the oxygen vacancy hypothesis and that we can increase their concentration by annealing in reduced oxygen atmosphere. Furthermore, we can not see a difference when the samples annealed in oxygen are annealed again in argon. It was previously claimed that an extra annealing in argon 'brings out' the oxygen vacancies, thus increasing the PL[45].
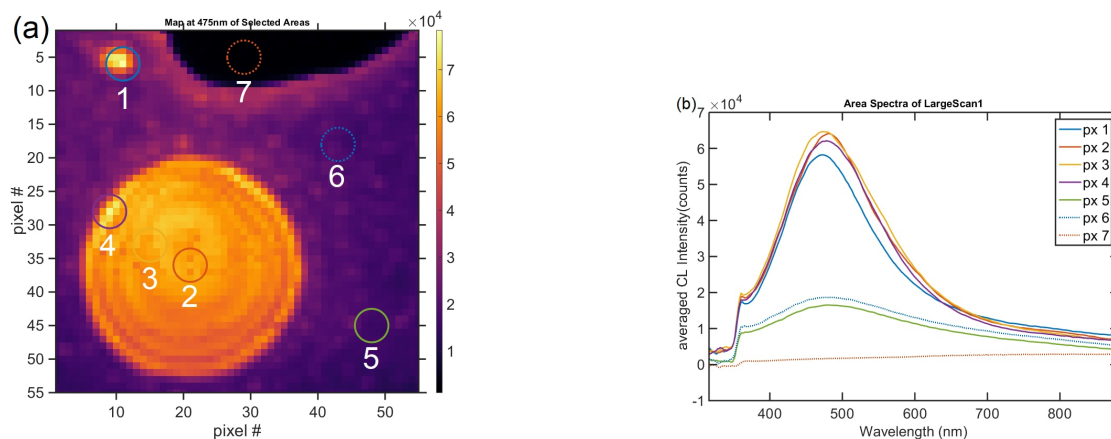
FIGURE 4.9: In (a) CL intensity map for 490 nm light, showing the locations of the taken spectra (9 pixels in each circle) and in (b) the spectrum corresponding to each location. One pixel is 8.64×8.64 nm. The sample used is the ZrO_2 sample annealed in the 10% oxygen atmosphere at 500°C for 2h.

Because the film has very distinct features, the spatial resolution that the CL setup provides us with is very interesting. We saw two distinct features in the films: holes and bubbles. We assumed that when crystallization starts at a specific point in the film, this can cause the film to tear. To check these assumptions we took measurements in the hole (dashed orange line, 7), on a small bubble (blue, 1), on the big bubble (purple, 4; yellow, 3 and orange, 2) and on the film (green, 5 and dashed blue, 6). We see one band at 490 nm for all locations except for the location in the hole, confirming that this is indeed a hole. The measurements on the bubbles have a significantly higher CL intensity than those on the film, confirming that these are crystallization centers.

4.3 hafnia

We would expect the PL in hafnia to
exhibit the same variance as zirconia in
luminescence with regards to the Oxy-
gen/argon ratio during annealing. Un-
fortunately the samples annealed at 10%
Oxygen pressure, gave a very different sig-
nal compared to the other samples. In PL
this resulted in a very 'clean' spectrum,
compared to the spectra in 4.10, making it
hard to make the same comparison as we
did for zirconia. We think the reason for
this, is that the surface morphology of the
10% film is far more homogeneous than
the other samples. We can see emission at
450 nm and emission that is largely cut-
off by our filter. It is however likely that
the band we see at 670 nm is the second
order of this emission, estimating it to be
at approximately 335 nm. The emission at
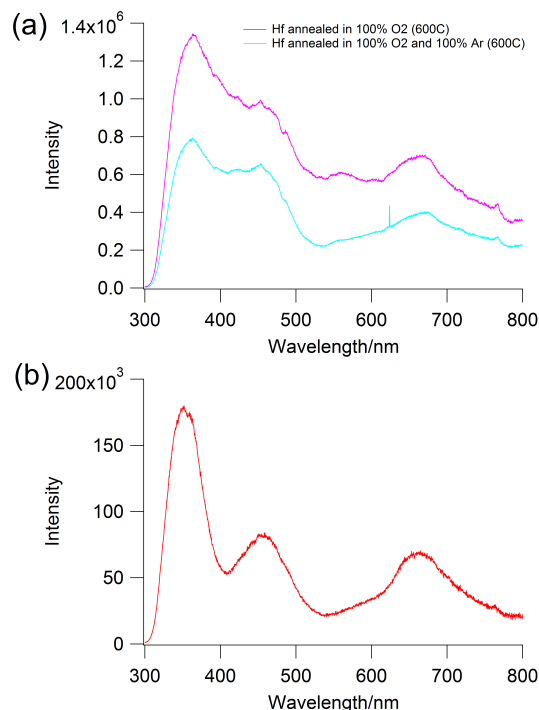450 nm is however the band that has been

FIGURE 4.10: In the top figure, the PL spectra
for the hafnia samples annealed in 100% oxygen
with (blue) and without (purple) extra annealing
in argon. In the bottom figure the spectrum for
the sample annealed in 10% Oxygen. Excitation
light is 220 nm and we use a long-pass filter at
330 nm.

found by various authors and assigned to oxygen vacancy related interactions[31][28].
Similarly to zirconia, we would expect this band to be relatively increased in the sample
annealed in 10% oxygen. This however is not the case, and the total PL signal is even or-
ders of magnitude smaller. This can have two reasons. As discussed in the introduction,
the shallow trap levels formed by the oxygen vacancies can act as quenchers, as well as
emission centers[35]. So it could be that the film has too many oxygen vacancies, so that
the PL signal decreased. On closer inspection this seems to not be the case however.
When we look with the microscope we see far less 'bubbles', as seen in de CL, than in
the samples annealed in 100% oxygen. This indicates that the crystallization process
has not advanced as far as in the other samples, causing the decrease in PL intensity.
So we suspect that during the annealing process there was a malfunction or mistake in
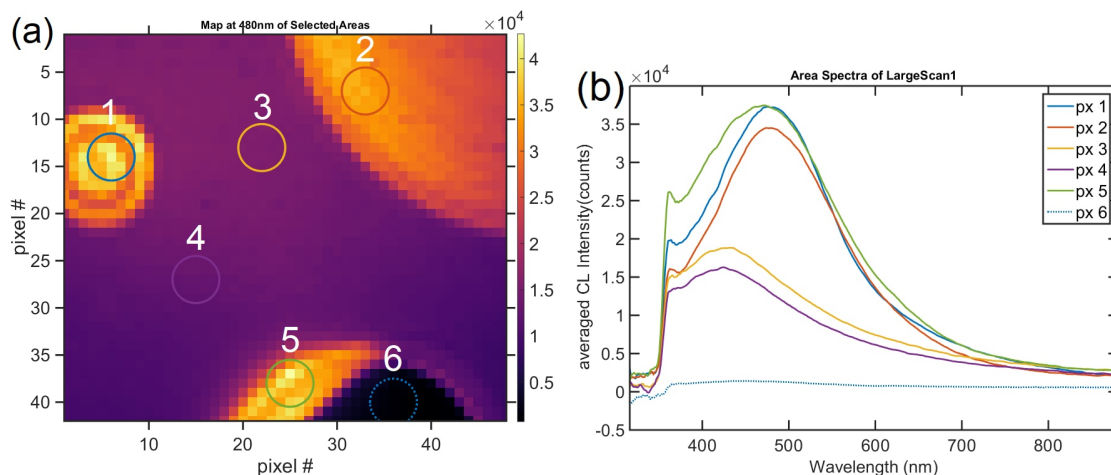the operation of the tube furnace.

FIGURE 4.11: In (a) CL intensity map for 490 nm light, showing the locations of the taken spectra (9 pixels in each circle) and in (b) the spectrum corresponding to each location. One pixel is 8.64×8.64 nm. The sample used is the HfO_2 sample annealed in the 10% oxygen atmosphere at 500°C for 2h.

In our CL-results, we see the same spatial features in hafnia as in zirconia. The film is rich in the bubbles and holes that we saw previously. We see a higher CL-signal coming from the bubbles than the measurements taken from the regular surface of the film, further asserting the hypothesis that the bubbles are centers of crystallization. The difference is that the 'regular' film emits at a lower wavelength than the bubbles. The spectra taken on the bubble (pixels 1, 2 and 5) show an emission band at 500 nm, while the spectra taken from the 'regular' surface (pixels 3 and 4) show emission at 420 nm. The 420 nm emission can be seen in the spectra from the bubbles as a shoulder on the main band. The logical explanation would be that the 420 nm emission belongs to metallic hafnium, although we cannot find any reference of pure metallic hafnium luminescence.

The Raman spectra from the hafnia and zirconia thin films, as presented in figure 4.12, resemble the spectrum of the substrate even more than the tin oxide samples. Besides this, they also suffer from a high background. Especially the zirconia samples exhibit a high background. Strangely, the samples from both materials that show significantly higher background, are not annealed with the same Oxygen/argon ratio. In the hafnia samples it is the sample annealed at 10% Oxygen, while in zirconia it is the samples annealed in Oxygen and subsequently in argon. We must therefore assert that the the raman signal coming from the hafnia and zirconia thin films is too small compared to the substrate to be able to draw any conclusions.
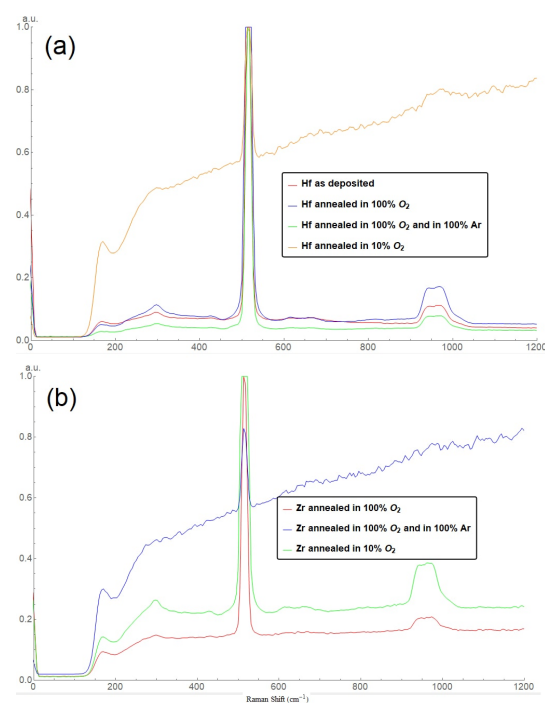

FIGURE 4.12: In the top figure the Raman spectrum of the various hafnia samples, from an accumulation time of 30s. In the bottom figure, the spectra of the various zirconia samples, from an accumulation time of 5s.

4.4   Nanoparticles

One of the main goals of this project was to compare the results of a bulk film with those of nanoparticles of the same material, as these types of nanopaticles are being tested and used in EUV lithography. In figure 4.13 we see the PL-spectra of the various nanoparticles in solution, with 220nm excitation. All samples show a broad PL peak, for hafnia the peak is centered at 343 nm, for zirconia at 425 nm and for tin oxide at 448 nm. hafnia
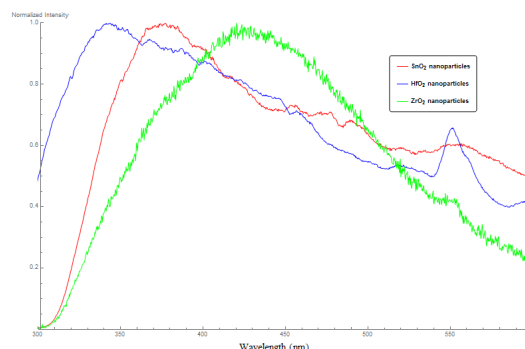

FIGURE 4.13: The PL spectra of the different kinds of nanoparticles, with 220 nm excitation light.

and zirconia also exhibit an additional peak at 551 and 545 nm respectively. In the theoretical introdution we mentioned a paper by Rauwel et al. [35], where pure cubic and pure monoclinic hafnia nanoparticles were fabricated. Their PL spectrum was composed of four peaks: 400, 442, 495 and 563 nm. In the monoclinic nanoparticles, the 495 peak is the dominant feature in the spectrum. In the cubic nanoparticles the spectrum is characterized by the 400, 442 and 495nm peaks. In our data we see a clear signal in the 400-500nm range, but the data is not clean enough to reliably distinguish these peaks. although similar peaks as mentioned by Rauwel et al. are definitely present. This probably depends on several factors, most likely the purity of the product.

Chapter 5

Conclusion

In conclusion, we have learned several things about the thin films synthesised here. For starters, the synthesis is far from trivial. When looking through the literature, authors have reported different emission bands, crystalline compositions and surface morphologies for seemingly similar deposition methods. The physical deposition methods used here, are apparently not optimal in determining the very specific properties we are looking for. The difference between the Hafnia and Zirconia samples annealed at 10% Oxygen for instance, is not easily explained. As we can see in the TEM pictures taken in the CL device, the films become very inhomogeneous after annealing. Concluding from the PL spectrum taken from the 'clean' Hafnia sample annealed at 10% Oxygen, this structural inhomogeneity is responsible for a noisier spectrum. The way to study these materials in the future most likely lies with Atomic-Layer-Deposition(ALD)-techniques, which have already been explored[46]. ALD should provide a structurally homogeneous film with a clearly defined crystal structure, which makes conclusions simpler and more reliable. The PL results confirmed what has been previously found, that annealing Hafnia and Zirconia films in an oxygen-poor atmosphere enhances the luminescence of bands associated with oxygen-vacancy-mediated electron processes. We could not make the same conclusion regarding the tin oxide films. The results were not clear enough to make any strong comparisons with the nanoparticle PL-data showed here. Once again improvement in synthesis and spectroscopy could improve the quality of the data. In eventual use of these materials in a lithography context, this should help determine some of the conditions of pre- and post-exposure bakes and provide insight in the actual lithography mechanisms.

Bibliography

[1] G.E. Moore. cramming more components onto integrated circuits. *Electronics*, 38 (8):114–117, 1965.

[2] V. B. Lopez Gejo F. Shluger A. L. Nieminen R. M. Foster, A. S. Sulimov. Structure and electrical levels of point defects in monoclinic zirconia. *Physical Review B*, 64 (22):224108, 2001.

[3] Z.C. Wu W.S. Hu, Z.G. Liu. Comparative study of laser ablation techniqes for fabricating nanocrystalline sno2 thin films for sensors. *Materials Letters*, 28:369–372, 1996.

[4] A.M. Serventi R. Dolbec, M.A. El Khakani. Microstructure and physical properties of nanostructured tin oxide thin films grown by means of pulsed laser deposition. *Thin Solid Films*, 419(1-2):230–236, 2002.

[5] R. Sathyamoorthy K.M. Abhirami and K. Asokan. Structural, optical and electrical properties of gamma irradiated sno thin films. *Radiation Physics and Chemistry*, 91:35–39, 2013.

[6] N. Kawai K. Suito. High pressure synthesis of orthorhombic sno_2. *Mater. Res. Bull.*, 10(7):677680, 1975.

[7] M. Batzill and U. Diebold. The surface and materials science of tin oxide. *Progress in Surface Science*, 79(2-4):47–154, 2005.

[8] Çetin Kiliç and Alex Zunger. Origins of coexistence of conductivity and transparency in sno_2. *Phys. Rev. Lett.*, 88(9):095501, 2002.

[9] M.K. L F. Gu, S.F. Wang. Luminescence of sno2 thin films prepared by spin-coating method. *Journal of Crystal Growth*, 262(1-4):182–185, 2004.

[10] C. Feng Song F. Gu, S. Fen Wang. Synthesis and luminescence properties of sno2 nanoparticles. *Chemical Physics Letters*, 372(3-4):451–454, 2003.

[11] W. Liu S. Luo, J. Fan. Synthesis and low-temperature photoluminescence properties of sno$_2$ nanowires and nanobelts. *Nanotechnology*, 17(6):1695–1699, 2006.

[12] A. Setaro S. Lettieri, M. Causa. Direct role of surface oxygen vacancies in visible light emission of tin dioxide nanowires. *The Journal of Chemical Physics*, 129(24): 244710, 2008.

[13] T. Oikawa T. Shimizu, T. Yokouchi. Contribution of oxygen vacancies to the ferroelectric behavior of hf0.5zr0.5o2 thin films. *Applied Physics Letters*, 106(11):112904, 2015.

[14] C.H. Cheng D.R. Islamov, V.A. Gritsenko. Origin of traps and charge transport mechanism in hafnia. *Applied Physics Letters*, 105(22):222901, 2014.

[15] F. Zeng G. S. Tang S. Z. Li C. Song H. D. Fu C. Chen, S. Gao and F. Pan. Migration of interfacial oxygen ions modulated resistive switching in oxide-based memory devices. *Journal of Applied Physics*, 114:014502, 2013.

[16] J. Sha W.J. Bae, M. Trikeriotis. High refractive index and high transparency hfo$_2$ nanocomposites for next generation lithography. *Journal of Materials Chemistry*, 20(25):5186, 2010.

[17] Y.S. Chung M. Trikeriotis, M. Krysak. Nanoparticle photoresists from hfo$_2$ and zro$_2$ for euv patterning. *Journal of Photopolymer Science and Technology*, 25(5): 583–586, 2012.

[18] C. Ouyang M. Krysak, M. Trikeriotis. Nanoparticle photoresists: Ligand exchange as a new, sensitive euv patterning mechanism. *Journal of Photopolymer Science and Technology*, 26(5):659–664, 2013.

[19] M. Trikeriotis B. Cardineau, M. Krysak. Tightly bound ligands for hafnium nanoparticle euv resists. *Proceedings of SPIE*, 8322:83220V–83220V–10, 2012.

[20] S.B. Erenburg T.V. Perevalov, A.A. Gritsenko. Atomic and electronic structure of amorphous and crystalline hafnium oxide: X-ray photoelectron spectroscopy and density functional calculations. *Journal of Applied Physics*, 101(5):053704, 2007.

[21] D. Panda T.Y. Tseng. Growth, dielectric properties, and memory device applications of zro$_2$ thin films. *Thin Solid Films*, 531:1–20, 2013.

[22] A. Li W. Liu, D. Wu. Annealing and doping effects on structure and optical properties of solgel derived zro$_2$ thin films. *Applied Surface Science*, 191:181–187, 2002.

[23] O. Robbe G. Ehrhart, B. Capoen. Structural and optical properties of npropoxide solgel derived zro$_2$ thin films. *Thin Solid Films*, 496(2):227–233, 2006.

[24] Y. Mao J.P. Chang J.H. Choi. Development of hafnium based high-k materialsa review. *Materials Science and Engineering: R: Reports*, 72(6):97–136, 2011.

[25] L.Q. Zhu G. He, M. Liu. Effect of postdeposition annealing on the thermal stability and structural characteristics of sputtered hfo$_2$ films on si (100). *Surface Science*, 576(1-3):67–75, 2005.

[26] G.A. Lopez C.V. Ramana, M. Vargas. Effect of oxygen/argon gas ratio on the structure and optical properties of sputter-deposited nanocrystalline hfo$_2$ thin films. *Ceramics International*, 41(5):6187–6193, 2015.

[27] E. Fortunato L. Pereira, P. Barquinha. Influence of the oxygen/argon ratio on the properties of sputtered hafnium oxide. *Materials Science and Engineering: B*, 118 (1-3):210–213, 2005.

[28] V.S. Aliev T.V. Perevalov, D.V. Gulyaev. The origin of 2.7 ev blue luminescence band in zirconium oxide. *Journal of Applied Physics*, 116(244109):11–15, 2014.

[29] Z. Li J. Ni, Q. Zhou. Oxygen defect induced photoluminescence of hfo$_2$ thin films. *Applied Physics Letters*, 93(1):2008–2010, 2008.

[30] S. Palmier A. Ciapponi, F.R. Wagner. Study of luminescent defects in hafnia thin films made with different deposition techniques. *Journal of Luminescence*, 129(12): 1786–1789, 2009.

[31] K. Nakamura T. Ito, M. Maeda. Similarities in photoluminescence in hafnia and zirconia induced by ultraviolet photons. *Journal of Applied Physics*, 97(5):054104– 054104–7, 2005.

[32] G. Zheng Z. Wang, J. Zhang. The unusual variations of photoluminescence and afterglow properties in monoclinic zro$_2$ by annealing. *Journal of Luminescence*, 132 (11):2817–2821, 2012.

[33] C. Chen S. Chuang, H. Lin. Oxygen vacancy relationship to photoluminescence and heat treatment methods in hafnium oxide powders. *Journal of Alloys and Compounds*, 534:42–46, 2012.

[34] C. Persson M.F. Sunding A. Galeckas P. Rauwel, E. Rauwel. One step synthesis of pure cubic and monoclinic hfo2 nanoparticles: Correlating the structure to the electronic properties of the two polymorphs. *Journal of Applied Physics*, 112(10): 1–9, 2012.

[35] A. Galeckas E. Rauwel and P. Rauwel. Photolumuinescent cubic and monoclinic hfo$_2$ nanoparticles. *Journal of Applied Physics*, 1:015035, 2015.

[36] G. Li G. He, Z. Sun. Review and perspective of hf-based high-k gate dielectrics on silicon. *critical reviews in solid state and materials sciences*, 37(3):131–157, 2012.

[37] Y. Mao J.H. Choi and J.P. Chang. Development of hafnium based high-κ materials– a review. *Materials Science and Engineering R*, 72(6):97–136, 2010.

[38] N.A. Geisse. Afm and combined optical techniques. *Materialstoday*, 12(7-8):4045, 2009.

[39] B. Berry. Probing light emission at the nanoscale with cathodoluminescence. *PhD Thesis*, 2016.

[40] B. Allieri F. Pioselli E. Comini G. Sberveglieri M. Zocchi L.Sangaletti, L.E. Depero. Oxidation of sn thin films to sno2. micro-raman mapping and x-ray diffraction studies luigi. *Journal of MATERIALS RESEARCH*, 13(9):2457–2460, 1998.

[41] Jianbing He Hongbo Fan Zhengxiu Shao Jianda Hong, Ruijin Huang. Influence of different post-treatments on the structure and optical properties of zinc oxide thin films. *Applied Surface Science*, 242(3-4):346–352, 2005.

[42] K. Asokan K.M. Abhirami, R. Sathyamoorthy. Structural, optical and electrical properties of gamma irradiated sno thin films. *Radiation Physics and Chemistry*, 91:35–39, 2016.

[43] P.B. Nair J.S. Lakshmi G.P. Daniel P.V. Thomas K. Joy, I.J. Berlin. Effects of annealing temperature on the structural and photoluminescence properties of nanocrystalline zro$_2$ thin films prepared by solgel route. *Journal of Physics and Chemistry of Solids*, 72(6):673–677, 2011.

[44] J.K. Thomas P.V. Thomas K. Joy I.J. Berlin, L. V. Maneeshya. Enhancement of photoluminescence emission intensity of zirconia thin films via aluminum doping for the application of solid state lighting in light emitting diode. *Journal of Luminescence*, 132(11):3077–3081, 2012.

[45] V. A. Pustovarov V. Sh. Aliev V. A. Gritsenko A. P. Yelisseyev E. V. Ivanova, M. V. Zamoryanskaya. Cathodo- and photoluminescence increase in amorphous hafnium oxide under annealing in oxygen. *Journal of Experimental and Theoretical Physics*, 120(4):710–715, 2015.

[46] J. Becker R.G. Gordon D.M. Hausmann, E. Kim. Atomic layer deposition of hafnium and zirconium oxides using metal amide precursors. *Chemistry of Materials*, 14(10):4350–4358, 2002.